Discussion of "Hydrodynamic Loading on River Bridges" by Stefano Malavasi and Alberto Guadagnini

November 2003, Vol. 129, No. 11, pp. 854–861.
DOI: 10.1061/(ASCE)0733-9429(2003)129:11(854)

Carlos V. Alonso[1]
[1]National Sedimentation Laboratory, Agricultural Research Service, U.S. Dept. of Agriculture, Oxford, MS.

The authors have made a very useful contribution to the understanding of hydrodynamic forces acting on submerged bridge decks approximated as rectangular cylinders. Based on their experimental findings and dimensional analysis, they provided relationships relating hydrodynamic loading coefficients to deck-Froude number and geometric-similarity parameters. In particular, an explicit form of the functional relationship between these parameters and the overall drag coefficient was developed from linear-momentum conservation considerations. This discussion is intended to supplement the authors' contribution by a closer examination of the behavior of drag loading when the circular cylinders interact with the free surface. As pointed out by the authors, results obtained for circular cylinders are not directly applicable to rectangular bridge decks. Nevertheless, the following analysis is useful in that it reveals the intrinsic wave-origin of that interaction, and highlights an alternate hydrodynamic path for arriving at the same parametric relationship developed by the authors.

A horizontal cylinder positioned beneath a free surface creates differences in the water-surface level around the body resulting in the formation of standing surface deformations. Lamb (1945) presented the first analysis of this phenomenon for the case of a two-dimensional, circular, stationary cylinder beneath the free surface of a steady, uniform, potential flow. He assumed the existence of an irrotational (potential) flow around a circular cylinder with diameter $D<z$, where z is the distance from the cylinder's axis to the undisturbed free surface. The free-surface displacement $\eta(x,t>0)$ about the undisturbed free surface, $\eta(x,0)=0$, where x is the streamwise distance from the vertical passing through the cylinder's axis and t is time, as developed by Lamb and normalized by the discusser, is given by

$$\eta^0 = \frac{1}{2}\frac{z^0}{(x^0)^2+(z^0)^2} - [\pi \mathsf{F}_r^{-2}\exp(-z^0/4\mathsf{F}_r^2)\sin(x^0/4\mathsf{F}_r^2)]\delta_x(x-0^+) \tag{1}$$

where $x^0=x/D$, $\eta^0=\eta/D$, $z^0=z/D$=cylinder submergence; $\mathsf{F}_r=U/\sqrt{gD}$=cylinder Froude number; U=velocity of the undisturbed uniform flow; g=gravitational acceleration; $\delta_x=\{0;1:x=0;>0\}$=Kronecker-delta definition; and 0^+ denotes the positive domain of the x-axis. Eq. (1) shows that there is a local free-surface disturbance immediately upstream of the cylinder, followed by a wave train that remains stationary with respect to the cylinder and decreases in amplitude and wavelength as the parameter $z^0/4\mathsf{F}_r^{-2}$ increases and F_r decreases, respectively (Fig. 1).

Lamb's solution requires that vorticity vanish everywhere—namely, it is predicated on the existence of an inviscid flow domain. On the other hand, it is well known that inviscid flow theory usually leads to acceptable approximations of viscous flows provided vorticity is confined to discrete points or thin sheets (Marshall 2001). This hypothesis is supported in the present case by the experiments reported by Sheridan et al. (1997). They found that flow past a circular cylinder beneath a free surface leads to near wake structures dominated by discrete vorticity layers whose pattern varies with the cylinder Froude number and submergence. Fig. 2 reproduces two of the wake states examined by Sheridan et al. for a submergence value of $z^0=0.9$. At $\mathsf{F}_r=0.60$ a mixing layer forms from the bottom of the cylinder and a jet-like flow separates from the top of the cylinder and remains attached to the free surface which exhibits a nearly periodic stationary wave of diminishing amplitude [Fig. 2(a)]. When the Froude number increases to $\mathsf{F}_r=0.97$, the jet-like flow separates from the free surface and is deflected downwards, merging with the lower mixing layer [Fig. 2(b)]. All the wake states examined by Sheridan et al.(1997) contain substantial regions of irrotational flow surrounding the mixing layers. This fact lends enough validity to Lamb's inviscid solution, and although he introduced the approximation $z>D$ to arrive at his results while $z<D$ in Fig. 2, the similarity between the free-surface shapes displayed in Figs. 1 and 2 is significant. It is further noted that inviscid theory cannot predict the onset of flow separation from the free surface that leads to the positive vorticity in the recirculation region between the jet and the free surface [Fig. 2(b)]. Thus, the downstream free-surface profile displayed in Fig. 1(b) should be related to the flow separation boundary, approximated by the dashed line in Fig. 2(b).

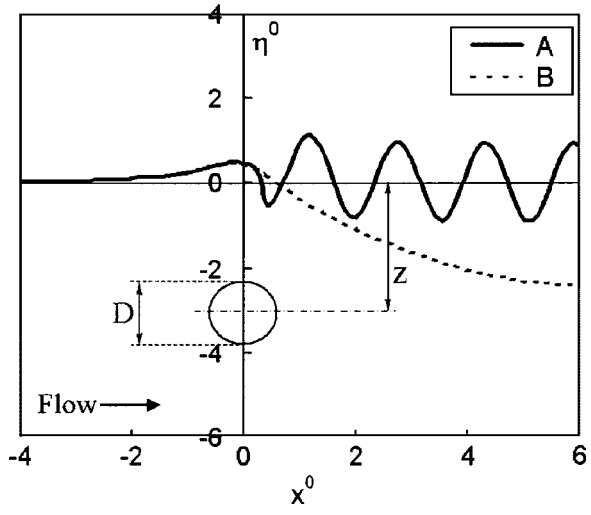

Fig. 1. Normalized free-surface shapes produced in a steady, uniform, inviscid flow by a submerged cylinder normal to the stream, after Lamb (1945). (A) $\mathsf{F}_r=0.50$, $z/D=1.0$; (B) $\mathsf{F}_r=1.0$, $z/D=1.0$. The dimensions z and D shown in the figure are not at scale and are shown for illustrative purposes only.

J. Hydraul. Eng. 2005.131:628-628.

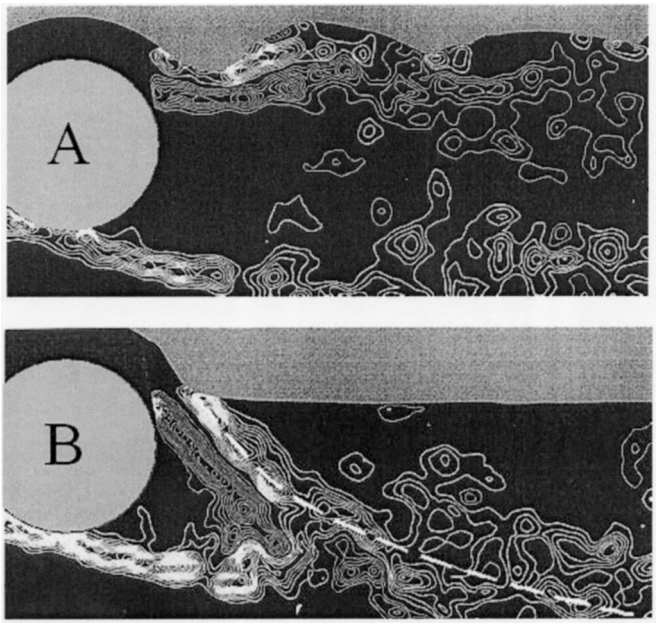

Fig. 2. Instantaneous free-surface shapes and vorticity fields around a submerged cylinder obtained by varying the cylinder Froude number at constant submergence. Vorticity fields were measured using laser-scanning particle-image velocimetry. The cylinder is represented by the solid gray circle; thick contours denote positive vorticity and thin contours are negative vorticity (adapted from Sheridan et al. 1997). (A) $F_r=0.60$, $z/D=0.9$; (B) $F_r=0.97$, $z/D=0.9$. The dashed white line roughly separates the jet-like structure emanating from the top of the cylinder and the recirculating zone above it.

A consequence of the foregoing mechanistic comparison, and the stated inviscid flow approximation notwithstanding, is that Lamb's analysis can be expected to provide adequate insight on the dynamic interaction between the body and the free surface. He arrived at an expression for the wave-drag force, f_w, per unit length of cylinder that can be reduced to the following dimensionless form:

$$\frac{4f_w}{g\rho_w\pi D^2}=\frac{\pi}{16}F_r^{-4}\exp(-z^0/2F_r^2) \tag{2}$$

where ρ_w represents the density of water. This force is the result of the pressure distributions within the inviscid flow domain, and does not account for the additional drag induced by energy dissipation within the shear layers of the near wake region. This force can be also expressed in the standard form:

$$f_w=C_wD\frac{\rho_wU^2}{2} \tag{3}$$

where C_w denotes the cylinder's wave-drag coefficient. Combining Eqs. (2) and (3) yields

$$C_w=\frac{\pi^2}{32}F_r^{-6}\exp(-z^0/2F_r^2) \tag{4}$$

This relationship shows that wave-drag depends on cylinder Froude number and submergence, a result similar to Eq. (7) derived by the authors for global drag from dimensional analysis considerations. It is also seen from Eq. (4) that wave drag increases exponentially as submergence decreases, vanishes at $F_r=0$, and decreases rapidly for $F_r\gg1$. Fig. 3 compares wave-drag coefficients computed with Eq. (4) with values of C_w obtained from the authors' data, which they kindly made available to the discusser. To this end, the wave-drag coefficient was computed by subtracting from the measured total-drag coefficients the drag coefficient for rectangular cylinders submerged in unbounded flows, i.e., $C_w=C_D-1.30$ (Blevins 1984).

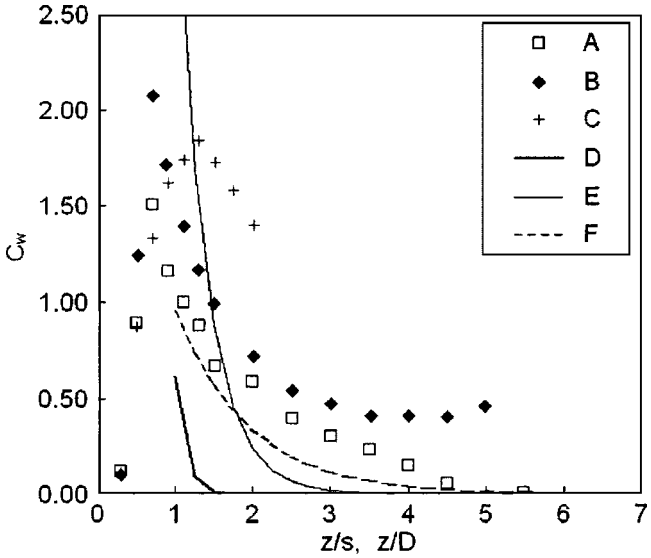

Fig. 3. Variation of wave-drag coefficient with cylinder Froude number and submergence. The markers represent data measured by the authors for (A) $F_r=0.26$; (B) $F_r=0.44$; and (C) $F_r=0.70$. The lines are variations predicted by Eq.(4) for (D) $F_r=0.26$; (E) $F_r=0.44$; and (F) $F_r=0.70$.

The parametric behavior predicted by Eq. (4) compares qualitatively well with the trends displayed by the measured coefficients. Previous work by Wallerstein et al. (2002) encountered a similar dependence of the wave drag for circular cylinders of finite length on Froude number and submergence. Fig. 3 shows that the only major departures between the theoretical and observed drag values occur for Froude numbers greater than 0.50, where the theory predicts a reverse in drag changes near the surface that is not reflected by the measurements, and for $z<D$, where the theory does not apply. However, the overall congruence of the functional forms yielded by both data and Eq. (4) for $z>D$ prompts the discusser to conclude that the variations of hydrodynamic drag loading recorded by the authors within the range $1<z/D<6$ is most likely dominated by the wave-drag phenomenon predicted by Lamb (1945). This conclusion is expected to hold as long as drag is not influenced by other parameters, such as the cylinder Reynolds number, its proximity to the channel bed, and its orientation with respect to the approaching flow (Alonso 2004).

Lamb (1945) indicated that his analysis for circular cylinders could be adapted to the case where the section of the cylinder has any arbitrary shape. The discusser is not aware whether this statement has been pursued elsewhere; if not, hydrodynamicists should be encouraged to extend Lamb's analysis to the case of rectangular cylinders studied by the authors.

J. Hydraul. Eng. 2005.131:628-628.

References

Alonso, C. V. (2004). "Transport mechanics of stream-borne logs." *Riparian Vegetation and Fluvial Geomorphology*, S. J. Bennett and A. Simon, eds., Water Science and Application 8, American Geophysical Union, Washington, D.C., 59–69.

Blevins, R. D. (1984). *Applied fluid dynamics handbook*, Van Nostrand Reinhold, New York, 309–347.

Lamb, H. (1945). *Hydrodynamics*, Dover, New York.

Sheridan, J., Lin, J. C., and Rockwell, D. (1997). "Flow past a cylinder close to a free surface." *J. Fluid Mech.*, 330, 1–30.

Wallerstein, N. P., Alonso, C. V., Bennett, S. J., and Thorne, C. R. (2002). "Surface wave forces acting on submerged logs." *J. Hydraul. Eng.*, 128(3), 349–353.

Marshall, J. S. (2001). *Inviscid incompressible flow*, Wiley, New York.

Discussion of "Hydrodynamic Loading on River Bridges" by Stefano Malavasi and Alberto Guadagnini

November 2003, Vol. 129, No. 11, pp. 854–861.
DOI: 10.1061/(ASCE)0733-9429(2003)129:11(854)

Mark A. Jempson[1] and Colin J. Apelt[2]

[1]Manager Victoria, WBM Oceanics Australia, P.O. Box 604, Collins St. West, Vic 8007, Australia. E-mail: majempson@wbmpl.com.au

[2]Professor Emeritus, Dept. of Civil Engineering, Univ. of Queensland, Brisbane Qld 4072, Australia. E-mail: c.apelt@uq.edu.au

The authors state their intention to compare their results for a bridge deck modeled as a cylinder of rectangular cross section with those in the literature on girder bridges. The discussers have carried out laboratory studies to determine hydrodynamic loads on models of eight types of real bridge decks. These were two variations of prestressed concrete girder bridges, a steel girder bridge, a spread box beam bridge, an adjacent box beam bridge, a steel truss bridge, a prestressed concrete deck unit bridge, and a box girder bridge. Time-averaged drag, lift, and moment coefficients were obtained for ranges of the Froude number of the flow, $\mathsf{F}=V_u/(gh_u)^{1/2}$, of the submergence ratio, $h^*=(h_u-h_b)/s$, and of the proximity ratio, $P_r=h_b/s$. The symbols here have the meanings given by the authors, i.e., V_u is the upstream mean flow velocity, g is gravity, h_u is the upstream flow depth, h_b is the height above the stream bed of the underside of the deck, and s is the overall thickness of the deck. Many of the results are given in Jempson and Apelt (1995, 1997), where the emphasis is on the development of codes for use by bridge designers. The complete sets of results are in Jempson (1994, 2000).

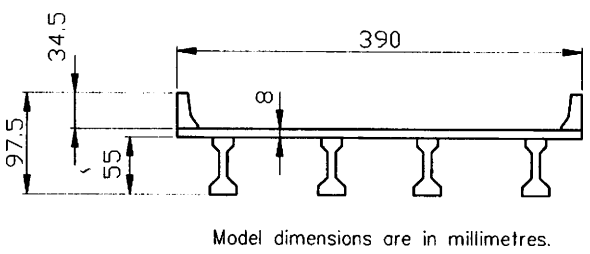

Fig. 1. Prestressed concrete girder bridge deck (Model scale 1:25)

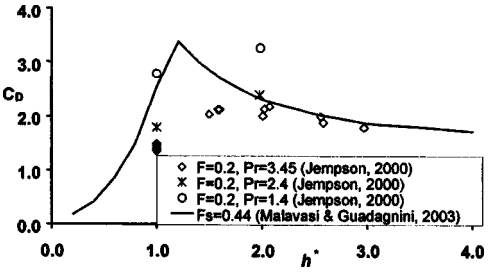

Fig. 2. Drag coefficients for prestressed concrete girder bridge deck model, compared with authors' results for deck with rectangular cross section

The authors have obtained force and moment coefficients as functions of h^* for constant values of the deck Froude number, $\mathsf{F}_s=V_u/(gs)^{1/2}$, whereas the discussers obtained these coefficients as functions of the flow Froude number, F. Unfortunately, the ratio between the two Froude numbers varies nonlinearly with h^* and it is not possible to make a direct comparison between the results. Nevertheless, a general comparison can be made. The discussers' most extensive studies were done for a prestressed concrete girder bridge, shown in Fig. 1. The ratio of length of cross section to overall height is 4. Some of the results for drag coefficient, C_D, and lift coefficient, C_L, are given in Figs. 2 and 3. The magnitude of F in these tests was 0.2. The nearest conditions in the authors' experiments are those for $\mathsf{F}_s=0.44$, for which F ranges from 0.24 at $h^*=1$ to 0.19 at $h^*=3$, and the authors' results for these conditions are included in Figs. 2 and 3 for comparison (these have been copied from the authors' Figs. 2 and 5). The authors' experiments were all done with the proximity ratio, P_r, constant at 2.33, while those of the discussers were mostly for $P_r=3.45$. The results obtained by the discussers at P_r values of 2.4 and 1.4 are included in Figs. 2 and 3. These illustrate the general result that C_D increases as P_r decreases, all else being the same.

Taking account of the differences in the deck shapes and in the test conditions, the data in Figs. 2 and 3 for the girder bridge and those for the rectangle show quite reasonable overall comparability, in general. The most obvious difference is that the sharp peak at $h^*=1.2$ in the authors' results for C_D is not present in the writers' data. In the latter, there is only a gradual maximum in the vicinity of $h^*=2$. This difference may be a consequence of the difference in shape. The model girder bridge had solid guardrails above the deck and girders below, and the shear layers separating from the upper and lower edges of these were large distances from the deck. In the case of the rectangular section tested by the

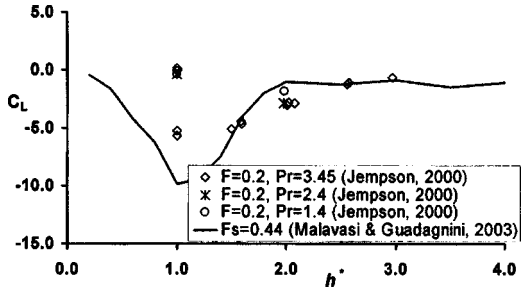

Fig. 3. Lift coefficients for prestressed concrete girder bridge deck model, compared with authors' results for deck with rectangular cross section

authors, the shear layers separated from the corners of the deck and the sharp peaks for C_D may be caused by interactions between these shear layers and the deck downstream.

The results obtained for moment coefficients have not been compared, as moments were referred to different centers.

The discussers are interested by the statement that the Federal Highway Administration (FWHA) (1995) suggested a constant value drag coefficient in the range 2 to 2.2, for use in design. Austroads (1992) recommended a drag coefficient of 2.2 for design. This was based on research that had been carried out in Queensland by Apelt (1986) and in a series of unpublished studies at the University of Queensland between 1986 and 1990. The detailed studies by the writers referred to in this discussion were carried out to obtain sufficient accurate data for better determination of design loads. The flood and debris design loads in the Australian bridge design standard (AS 2004) are based on this data.

Notation

The following symbols are used in this discussion:

C_D = drag coefficient;
C_L = lift coefficient;
F = Froude number of the flow;
F_s = deck Froude number;
g = gravity;
h_b = height above the stream bed of the underside of the bridge deck;
h_u = upstream flow depth;
h^* = $(h_u - h_b)/s$, the submergence ratio;
V_u = upstream mean flow velocity; and
P_r = h_b/s, the proximity ratio.

References

Apelt, C. J. (1986). "Flood forces on bridges." *Proc., 13th ARRB-5thREA Combined Conf., Adelaide, Aug. 1986*, Australian Road Research Board, Melbourne, Australia, 40–46.

Australian Standards (AS). (2004). "AS 5001.2, Bridge design, Part 2: Design loads." Melbourne, Australia.

Austroads. (1992). "92' AUSTROADS bridge design code." Austroads, Sydney, Australia.

Federal Highway Administration (FWHA). (1995). "Stream stability at highway structures." *Rep. No. FWHA-HI-96-032*, FHWA, Washington, D.C., 56–59.

Jempson, M. A. (1994). "Hydrodynamic forces on partially and fully submerged bridge superstructures." MEngSc thesis, Univ. of Queensland, Australia.

Jempson, M. A. (2000). "Flood and debris loads on bridges." PhD thesis, Univ. of Queensland, Australia.

Jempson, M. A., and Apelt, C. J. (1995). "Flood loads on bridge superstructures." *Proc., Bridges into the 21st Century*, Hong Kong, 2–5 Oct 1995, Hong Kong Inst. of Engineers, Hong Kong, 1025–1032.

Jempson, M. A., and Apelt, C. J. (1997). "Flood loads on submerged and semi-submerged bridge superstructures." *Proc., Bridging the Millenia* (Austroads 1997 Bridge Conf. Sydney, 3–5 Dec. 1997), G. J. Chirgwin, ed., Austroads, Inc., Sydney. 2, 19–33.

Closure to "Hydrodynamic Loading on River Bridges" by Stefano Malavasi and Alberto Guadagnini

November 2003, Vol. 129, No. 11, pp. 854–861.
DOI: 10.1061/(ASCE)0433-9429(2003)129:11(854)

Stefano Malavasi[1] and Alberto Guadagnini[2]

[1]Assistant Professor, Dipt. Ingegneria Idraulica, Infrastrutture Viarie, Ambientale, Rilevamento, Politecnico di Milano, Piazza Leonardo Da Vinci, 32, 20133 Milano, Italy. E-mail: stefano.malavasi@polimi.it

[2]Professor, Dipt. Ingegneria Idraulica, Infrastrutture Viarie, Ambientale, Rilevamento, Politecnico di Milano, Piazza Leonardo Da Vinci, 32, 20133 Milano, Italy. E-mail: alberto.guadagnini@polimi.it

We appreciate the interest of the discussers in our work and thank the discussers for their comments.

We agree with the motivations upon which Alonso (2005) bases his proposed extension of Lamb's analysis to rectangular cylinders. The rectangular and circular shapes lead to different mechanisms governing the vortex shedding. The results provided by Alonso (2005) contribute to interesting insights on the influence of the free surface on the hydrodynamic loading of the rectangular cylinder by means of an elegant analytical approach. Specifically, his Fig. 3 contrasts the wave drag coefficient calculated by means of the Lamb analysis with the drag coefficient obtained upon subtracting the drag coefficient of the unbounded condition, $C_D = 1.3$ (as suggested by Blevins 1984), from our experimental values (which were measured under bounded conditions). In order to fully understand the observed process, one should note that the experimental data of Malavasi and Guadagnini (2003) have been collected for different blockage ratios. The blockage ratio, γ_b, is defined as the ratio between the frontal area of the bridge deck that is impacted by the free surface stream and the total area of the free-surface stream measured at the reference section upstream of the bridge. This implies that the data reported by Alonso (2005) in his Fig. 3 can be considered as independent of

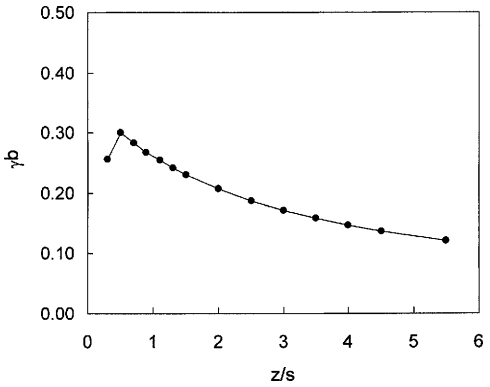

Fig. 1. Blockage ratio (γ_b) versus z/s calculated for the experimental data considered in Fig. 3 of the discussion

J. Hydraul. Eng. 2005.131:628-628.

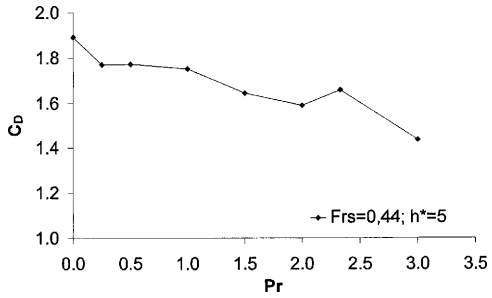

Fig. 2. The drag coefficient, C_D, versus the proximity ratio, Pr, for bridge deck modeled by a rectangular cylinder with an aspect ratio $1/s=3$ ($h^*=5$; $F_S=0.44$)

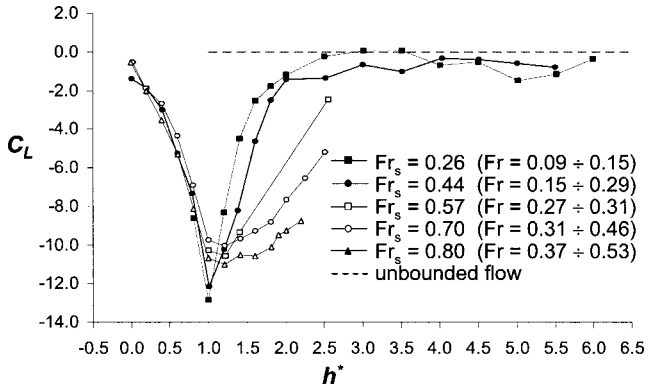

Fig. 5.

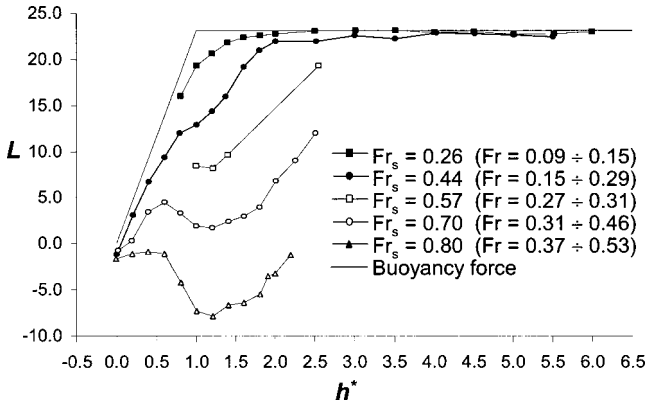

Fig. 7.

γ_b only for low values of this parameter. Fig. 1 depicts the influence of the blockage ratio on the experimental data considered by Alonso (2005). It reveals that an increase in the blockage ratio might cause the drag coefficient to increase. This feature has also been reported by Okajima et al. (1997) for symmetric bounded flow.

Two main points are raised by Jempson and Colin (2004): (1) they state that the drag coefficient, C_D, increases as the proximity ratio, Pr, decreases; and (2) their experiments performed on girder bridge decks (their Fig. 2) do not display a sharp peak for C_D at $h^* \approx 1.2$.

We do agree with their assessment of the dependence of C_D on Pr. We are now in a position to actively contribute to their comment. Fig. 2 depicts the dependence of measured C_D on Pr for a set of new experiments, recently performed using the same experimental setup of Malavasi and Guadagnini (2003) and $h^*=5$, $F_S=0.44$.

With regard to the second point, Jempson and Apet (2004) state that the different behavior of C_D might be due to the different deck shapes they analyze. It appears that the discussers base their assessment on data that were measured for Froude number $F=0.2$, and correspond to a range of deck Froude number $0.3 \leqslant F_S \leqslant 0.5$ (see Fig. 2 of the discussion of Jempson and Apet, 2004). In this range, F_S affects the drag coefficient values significantly, as shown by Malavasi and Guadagnini (2003, their Fig. 2). We also note that Fig. 3 of Malavasi and Guadagnini (2003) reports experimental values (Denson 1982; Tainsh 1965) that indicate the presence of a peak of C_D also for girder bridge decks, whose shape is very close to that analyzed by the discussers. We do agree with the comment of Jempson and Apet (2004) about the differences in the nature of shear layers/separation from the bridge deck edges for rectangular and girder deck.

Errata

The following corrections should be made to the original paper:

On page 858, Figs. 5 and 7 should be substituted for Figs. 5 and 7 presented here.

In the right column on page 858, the sentence on the fifth line should read "After that, the values of C_L do not change significantly; this is also corroborated by the significant uncertainty associated to the lift coefficient (Fig. 6)." In the ninth line of the same column, the words: "and does not appear to trend toward an asymptotic limit" should be deleted. Also, in the right column, the sentence starting on the twelfth row: "This appears more evident for the lift coefficient, which is much more sensitive to the asymmetric flow conditions than the drag coefficient" should be deleted.

References

Alonso, C. V. (2005). "Discussion of 'Hydrodynamic loading on river bridge.'" *J. Hydraul. Eng.*, 131(7), 619–621.

Blevins, R. D. (1984). *Applied fluid dynamics handbook*, Van Nostrand Reinhold, New York.

Denson, K. H. (1982). "Steady-state drag, lift and rolling-moment coefficients for inundated inland bridges." *Rep. MSHD-RD-82-077*, National Technical Information Service, Springfield, Va., 1–23.

Jempson, M. A., and Apet, C. J. (2004). "Discussion of 'Hydrodynamic loading on river bridge.'" *J. Hydraul. Eng.*, 131(7), 621–622.

Malvasi, S., and Guadagnini, A. (2003). "Hydrodynamic Loading on River Bridge." *J. Hydraul. Eng.*, 129(11), 854–861.

Okajima, A., Yi, D., Kimura, S., and Kiwata, T. (1997). "The blockage effect for an oscillating rectangular cylinder at moderate Reynolds number." *J. Wind. Eng. Ind. Aerodyn.*, 69–71, 997–1011.

Tainsh, J. (1965). "Investigation of forces on submerged bridge beams." *Rep. No. 108*, Dept. of Public Works, New South Wales Univ., Sydney, Australia.

J. Hydraul. Eng. 2005.131:628-628.

Discussion of "Measurements of Sediment Erosion and Transport with the Adjustable Shear Stress Erosion and Transport Flume," by Jesse D. Roberts, Richard A. Jepsen, and Scott C. James

November 2003, Vol. 129, No. 11, pp. 862–871.
DOI: 10.1061/(ASCE)0733-9429(2003)129:11(862)

Mohammad Alkhalidi[1] and Ashish J. Mehta[2]
[1]Assist. Professor, Dept. of Civil Engineering, Kuwait Univ., P.O. Box 5969, Safat 13060, Kuwait.
[2]Professor, Dept. of Civil and Coast. Engineering, Univ. of Florida, Gainesville, FL 32611.

Introduction

The authors have raised the important issue of bedload and suspended load as functions of particle size d. In Fig. 5 they provide experimental evidence to support previous data which indicate that bedload will decrease from the nearly full (95%) to negligible (5%) fraction of the total load as particle size decreases from about 200 μm to 50 μm. The data of Mantz (1977) on the extension of the Shields curve using cohesionless particles finer than 50 μm are a useful adjunct to this analysis. In Fig. 5 one may notionally include the 0% bedload curve (Fig. 1), whose exact shape remains unknown but which can be expected to intersect the Shields curve at 20 μm, marking the onset of significant cohesion (Lee and Mehta, 1997). Fig. 1 also provides a qualitative understanding of the linkage between formulas for cohesionless and cohesive (<20 μm) sediment erosion fluxes. We will explore this issue briefly by using concepts well known in sediment transport.

Entrainment as a Function of Particle Size

The potential energy of a particle of diameter d entrained at a small height z_a above the bed is

$$\alpha_1 d^3 g(\rho_s - \rho)(z_a - k_s) \tag{1}$$

where g=acceleration due to gravity; ρ_s=particle density; ρ=fluid density; k_s=bed roughness; and α_1=particle volume shape factor. The shear work done to raise the particle to z_a is

$$\alpha_2 d^2(\tau_b - \tau_c)d \tag{2}$$

where τ_b=bed shear stress; τ_c=critical shear stress for erosion; and α_2=particle area shape factor. At equilibrium (for cohesionless sediment), we may equate the above two quantities and obtain

$$z_a = \frac{\alpha_2}{\alpha_1}\frac{(\tau_b - \tau_c)}{\rho g\left(\frac{\rho_s}{\rho} - 1\right)} + k_s \tag{3}$$

which can be restated as

$$\frac{z_a}{d} = \frac{\alpha_2}{\alpha_1}(\theta - \theta_c) + \frac{k_s}{d} \tag{4}$$

In the above expression, the Shields parameter θ and its critical value θ_c are given as

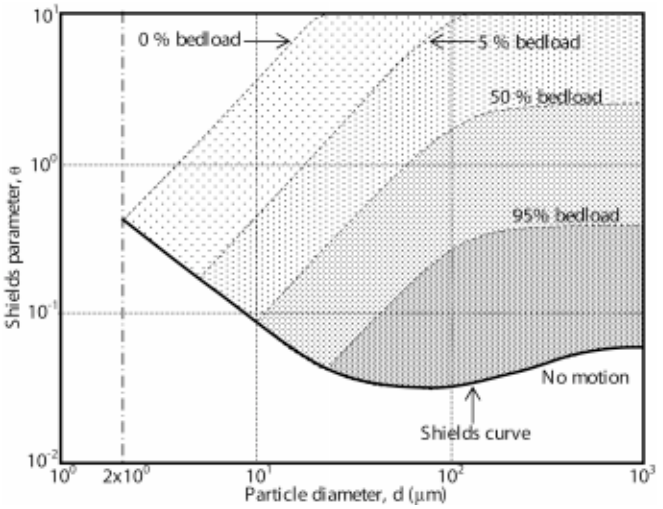

Fig. 1. Generalized entrainment diagram

$$\theta = \frac{\tau_b}{\rho g\left(\frac{\rho_s}{\rho} - 1\right)d}; \quad \theta_c = \frac{\tau_c}{\rho g\left(\frac{\rho_s}{\rho} - 1\right)d} \tag{5}$$

Assuming for our purpose $k_s/d=1$, Eq. (4) becomes

$$z_a - d = \frac{\alpha_2}{\alpha_1}(\theta - \theta_c)d \tag{6}$$

Now we may conveniently take θ_c to be associated with the Shields curve and θ to any of the bedload percent curves (Fig. 1). For example, taking the zero percent curve, we observe from Eq. (6) that the thickness of the bedload layer decreases with decreasing d and becomes zero at $z_a=d=20$ μm.

The bed particle entrainment flux q_e is obtained from, for instance, the formula

$$q_e = \frac{\gamma_a C_{z_a}\left(\frac{\tau_b - \tau_c}{\tau_c}\right)}{1 + \gamma_a\left(\frac{\tau_b - \tau_c}{\tau_c}\right)} \tag{7}$$

where C_{z_a}=reference concentration at z_a, and γ_a is a constant (McLean 1985). A heuristic interpretation of Eq. (7) for cohesive sediment is as follows. For $d \leqslant 20$ μm, z_a is equal to d, and C_{z_a} can be interpreted as the concentration of cohesive flocs that are recently detached from the bed. So for a given bed density, C_{z_a} and, therefore, $\gamma_a C_{z_a}=M$ can be taken as constants. The quantity γ_a scales with the settling velocity, which is on the order of 10^{-4} to 10^{-5} m/s for cohesive sediment. Moreover, the ratio $(\tau_b - \tau_c)/\tau_c$ is of the order 10^0 to 10^2. So we may assume $\gamma_a(\tau_b - \tau_c)/\tau_c \ll 1$ and Eq. (7) becomes

$$q_e = M\left(\frac{\tau_b - \tau_c}{\tau_c}\right) \tag{8}$$

which was first obtained for cohesive sediment erosion by Kandiah (1974).

References

Kandiah, A. (1974). "Fundamental aspects of surface erosion of cohesive soils." PhD thesis, Univ. of California, Davis, Calif.

Lee, S.-C., and Mehta, A. J. (1997). "Problems in characterizing dynamics of mud shore profiles." *J. Hydraul. Eng.*, 123(4), 351–361.
Mantz, P. A. (1977). "Incipient transport of fine grains and flakes by fluids—extended Shields diagram." *J. Hydraul. Div., Am. Soc. Civ. Eng.*, 103(6), 601–615.
McLean, S. R. (1985). "Theoretical modeling of deep sediment transport." *Mar. Geol.*, 66, 243–265.

Discussion of "Investigation on the Stability of Two-Dimensional Depth-Averaged Models for Bend-Flow Simulation" by T. Y. Hsieh and J. C. Yang

August 2003, Vol. 129, No. 8, pp. 597–612.
DOI: 10.1061/(ASCE)0733-9429(2003)129:8(597)

K. Blanckaert[1]
[1]Research Associate, ICARE-ENAC, Ecole Polytechnique Fédérale Lausanne, CH-1015 Lausanne, Switzerland

With the recent tendency to rehabilitate rivers, bends have received increased attention. Flow and morphology in river bends are largely determined by the secondary flow (also called spiral flow or helical flow), which is a characteristic feature that redistributes the velocity, the boundary shear stress, and the sediment transport. Contrary to three-dimensional numerical models, conventional depth-averaged two-dimensional (2D) models are intrinsically unable to account for the effects of the secondary flow: all information concerning the vertical flow structure is lost in the depth-averaging procedure. Quasi-three-dimensional models, called bend models by the authors, remedy this shortcoming by supplementing the 2D flow model with a closure submodel for the secondary flow. In the authors' terminology, this closure submodel provides the dispersion stresses to the 2D code. The authors' estimation of the range of validity of conventional 2D models, which are commonly used in engineering practice by comparing it to a bend model, is of engineering relevance.

The authors' study is exclusively based on simulations of flow in a 90° bend of constant curvature, preceded and followed by straight reaches, and with rectangular cross section. Whereas the choice of a single-bend configuration can be endorsed, the discusser considers the rectangular cross section as irrelevant for the purpose of the study. Hereafter, the fundamental difference between the physics of curved flow in rectangular and natural-like cross sections, and the implications for the numerical modeling of curved flows are discussed.

The discusser has carried out experiments in a strongly curved single-bend laboratory flume, which is 1.3 m wide and consists of a 9-m long straight inflow, followed by a 193° bend with constant centerline radius of curvature of $r_c = 1.7$ m, and a 5-m long straight outflow reach. The experimental setup and the hydraulic conditions of the experiments are shown in Fig. 1. The first experiment was carried out over a horizontal sand bed that was fixed by spraying paint on it. The second experiment adopted similar hydraulic conditions over a mobile sand bed. Imposition of a sediment discharge of 0.023 kg/ms lead to the pronounced bar-pool bed topography shown in Fig. 1. For the horizontal-bed experiment, detailed three-dimensional (3D) flow measurements were carried out in the 13 cross sections along the flume indicated in Fig. 1. For the developed-bed experiment, the presented velocity distributions are obtained by means of simulations with a 3D standard k-ε numerical model. Detailed velocity measurements are being carried out and will soon be reported.

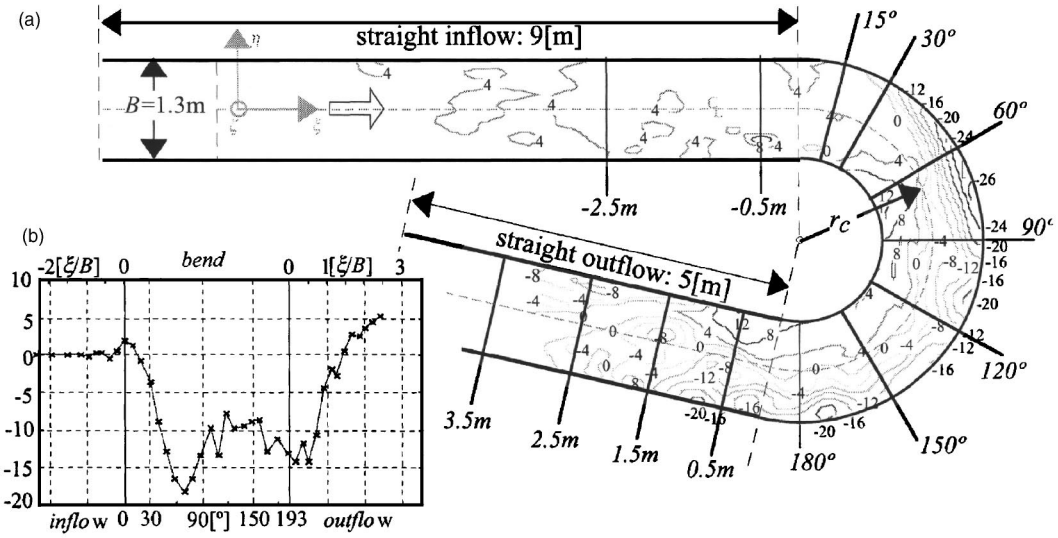

bed topo	Q [l/s]	q_s [kg/ms]	H [m]	U [m/s]	u_* [m/s]	$1/\sqrt{C_f}$ [/]	$\mathbf{R}=UH/\nu$ [/]	$\mathbf{F}$ [/]= $U/(gH)^{1/2}$	r_c/B [/]	r_c/H [/]	B/H [/]
hor.	89	0	0.159	0.43	0.040	10.8	69.000	0.35	1.31	10.6	8.2
nat.	89	0.023	0.163	0.42	0.054	7.8	68.000	0.33	1.31	10.4	8.0

Fig. 1. (a) Experimental flume, bed topography (in cm) referred to overall mean bed level, and measuring sections; (b) evolution of transversal bottom slope around the flume; and Table: hydraulic conditions

J. Hydraul. Eng. 2005.131:628-628.

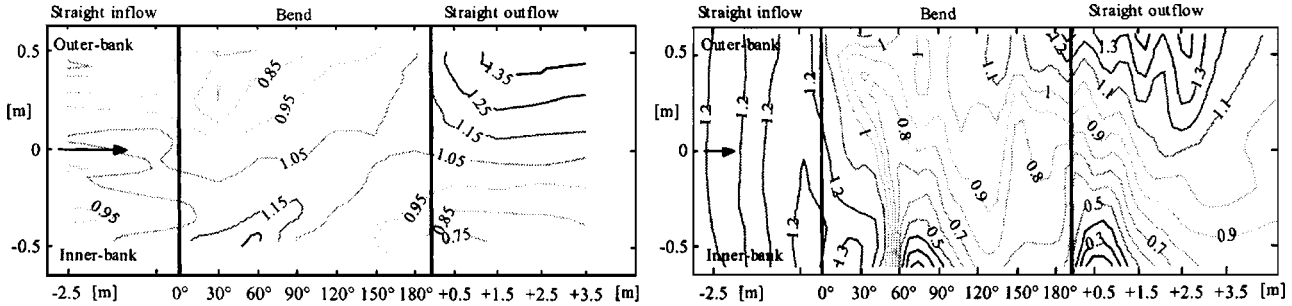

Fig. 2. Distribution of the normalized depth-averaged downstream velocity, $\bar{u}/U$, measured over horizontal (left) and simulated by means of standard 3D k-ε model over natural (right) bed topography

Fig. 2 illustrates the fundamentally different distributions of the depth-averaged downstream velocity in both experiments. Upon entering the bend, the core of maximum velocity moves toward the inner bank in both cases. Over the horizontal bed, it subsequently shifts gradually in outward direction, to reach the outer bank only near the bend exit. Over the developed bed, the core of maximum velocity has already crossed to the outer bank at 60°, and subsequently remains there.

Three major processes are responsible for these velocity (redistributions):

1. At the bend entry/exit, the sudden build-up/decay of the superelevation (transverse tilting of the water surface) due to the discontinuity in centerline curvature goes along with pronounced downstream water surface slopes. These cause significant accelerations/decelerations at the inner/outer bend near the bend entry and inverse at the bend exit.
2. The varying bed topography causes a redistribution of the flow, since the velocity tends to be higher/lower in deeper/shallower parts of the bend.
3. Due to so-called differential advection, the secondary flow causes a gradual outward shift of the core of maximum velocity.

These three processes are clearly discernable in the depth-averaged downstream momentum Eq. (2) of the paper, which can be reduced for steady flow in a reference system with only a curvilinear downstream axis (Blanckaert and de Vriend 2003)

$$\frac{\tau_{b1}}{\rho} = C_f \bar{u}\sqrt{\bar{u}^2+\bar{v}^2} = -\frac{gd}{h_1}\frac{\partial(z_b+d)}{\partial\xi} - \left(\frac{\bar{u}d}{h_1}\frac{\partial\bar{u}}{\partial\xi} + \bar{v}d\frac{\partial\bar{u}}{\partial\eta} + \frac{\bar{u}\bar{v}d}{h_1 r_c}\right) + \frac{1}{\rho h_1}\frac{\partial T_{11}}{\partial\xi} + \frac{1}{\rho}\frac{\partial T_{12}}{\partial\eta} + \frac{2}{\rho h_1}\frac{T_{12}}{r_c} \quad (1)$$

where $h_1=1+\eta/r_c$ and $h_2=1$. Both conventional 2D and bend models account for the first two processes, which are governed by the driving gravity term, $-h_1^{-1}gd\partial(z_b+d)/\partial\xi$. Only the bend model, however, accounts for the dispersion stresses, included in the effective stresses T_{ij} $(i,j=1,2)$. Blanckaert and Graf (2004) have shown that the dispersion stress contribution to the term $\partial T_{12}/\partial\eta$ represents the dominant secondary flow effect with respect to the velocity redistribution.

Over a natural-like developed bed, the secondary flow and the bed topography have a dominant influence on the velocity redistribution and are of comparable magnitude (Johannesson and Parker 1989). But the bed topography effects strengthen with increasing curvature, whereas the secondary flow effect weakens, which can be explained as follows: with increasing curvature, the transversal tilting of the bed increases, since it is roughly proportional to the secondary flow strength (Olesen 1987), causing a more pronounced outward skewing of the velocity distribution. Blanckaert and de Vriend (2003) have shown that the secondary flow effect depends on the spanwise velocity distribution. It is maximum when the core of maximum velocity occurs near the inner bank, and decreases when the core of maximum velocity shifts in an outward direction (cf. Fig. 5). Over a horizontal bed, however, the outward redistribution in the bend is exclusively due to the secondary flow. Thus, conventional 2D models that do not account for the secondary flow may yield acceptable results for flow over developed bed topography in sharp bends, where the bed topography effect dominates over the secondary flow effect. Over a horizontal bed, however, conventional 2D models will predict a fundamentally erroneous flow pattern, with the core of maximum velocity remaining near the inner bank all around the bend. Simulations of both experiments with a conventional 2D model (Blanckaert et al. 2003), shown in Fig. 3, illustrate these findings.

The authors' results comply with the above remarks. They find maximum relative errors in the predicted velocity distribution of $\mathrm{Max}U^* > 100\%$ for bends of moderate curvature (Figs. 1–3 in the

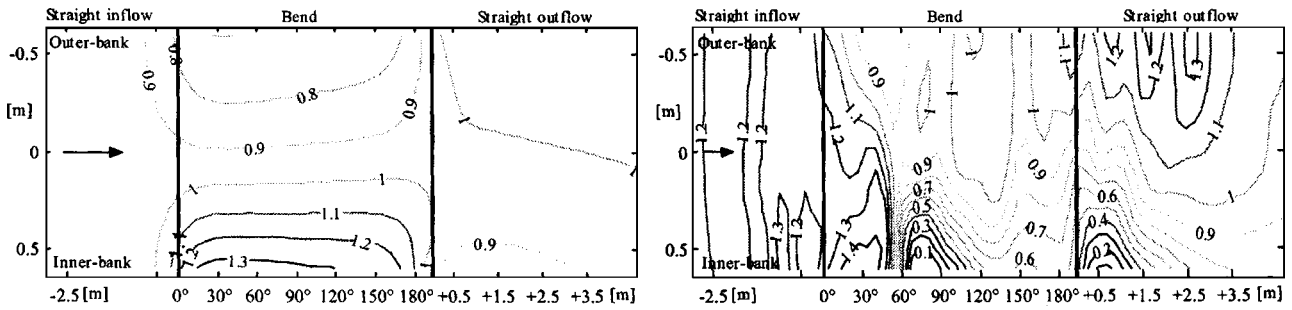

Fig. 3. Distribution of the normalized depth-averaged downstream velocity, $\bar{u}/U$, over horizontal (left) and natural (right) bed topography, simulated by means of a conventional two-dimensional model

J. Hydraul. Eng. 2005.131:628-628.

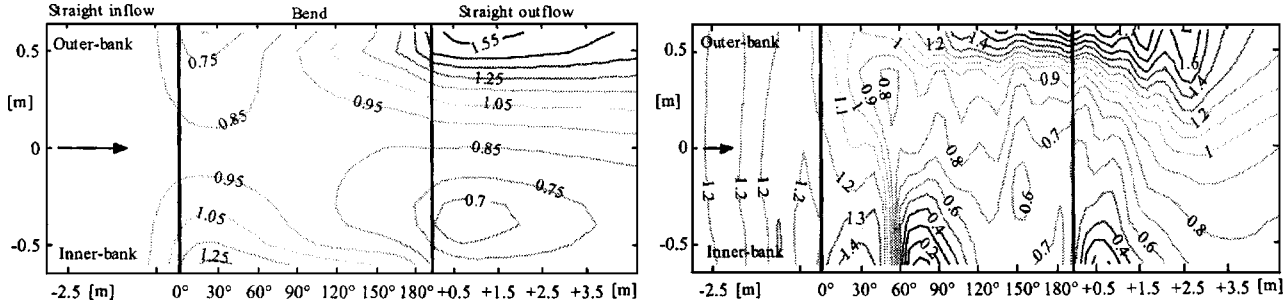

Fig. 4. Distribution of the normalized depth-averaged downstream velocity, $\bar{u}/U$, over horizontal (left) and natural (right) bed topography, simulated by means of a bend model

paper). For the discusser's sharp-bend experiments, characterized by *SI* values of 1.0 (horizontal bed) and 0.75 (developed bed), the authors indicate a relative error of $\mathrm{Max}U^{*} \sim 300\%$ (Fig. 2 in the paper). Moreover, they find that conventional 2D models are only suitable for a short range in the channel bend of de Vriend and Koch (1977), which is very weakly curved.

For the above reasons, the discusser believes that conventional 2D models may eventually be useful for flow in sharp bends over developed bed topography, but are fundamentally unsuitable for curved flows over horizontal bed topography, which necessitate at least a bend model.

Fig. 4 shows simulations of the discusser's experiments by means of a bend model, which is explained in detail by Blanckaert et al. (2003). Contrary to the conventional 2D models, this model captures the outward shift of the core of maximum velocity over the horizontal bed. For both configurations, the velocity redistribution by the secondary flow seems to be overestimated, and this to the point that the bend model does not perform better than the conventional 2D model for the developed bed case (cf. Figs. 2–4 of this discussion). This observation suggests that conventional 2D models may yield acceptable results for sharply curved flow over developed bed topography.

De Vriend (1981) has attributed the overestimation of secondary flow effects to the neglect of feedback between the downstream velocity and the secondary flow in the dispersion stress model [Eqs. (7)–(9)]. Experimental data by Blanckaert (2001, 2002) show that this overestimation can be as large as an order of magnitude for sharp bends. Blanckaert and de Vriend (2003, 2004) have investigated the mechanisms underlying the secondary flow and proposed a dispersion stress model that accounts for these feedback effects. Basically, it multiplies the dispersion stresses calculated according to Eqs. (7)–(9) with the correction factor I/I_0, shown in Fig. 5, which represents the ratio of secondary flow strength calculated with/without accounting for the feedback effects.

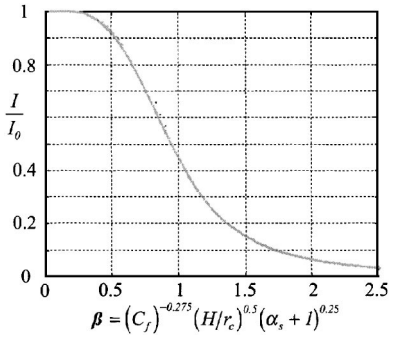

Fig. 5. Correction factor to the dispersion stress model, Eqs. (7)–(9), in order to account for feedback effects between the downstream velocity and the secondary flow

This correction factor uniquely depends on the so-called bend parameter $\beta = (C_f)^{-0.275}(H/r_c)^{0.5}(\alpha_s+1)^{0.25}$, where $\alpha_s = (\partial\bar{u}/\partial\eta)/(\bar{u}/r_c)$ parametrizes the width-distribution of the downstream velocity. Note that the bend parameter encompasses the relative strength of the secondary flow, $SI = (C_f)^{-0.5}(H/r_c)$ defined by the authors. Blanckaert et al. (2003) have obtained significantly improved simulations of both presented experiments by taking this correction factor into account.

The discusser would like to make two more remarks on the authors' modeling of the dispersion stresses:

1. The width-distribution of the dispersion stresses according to Eqs. (7)–(9) does not adequately represent the effects of the secondary flow cell, as discussed by Blanckaert (2001).
2. The authors' model neglects the inertial adaptation of the secondary flow to curvature changes. This leads to discontinuities in the dispersion stresses at the bend entrance and exit, and furthermore to their overestimation in the bend.

References

Blanckaert, K. (2001). "Discussion of 'Bend-flow simulation using 2D depth-averaged model' by H. C. Lien, et al.." *J. Hydraul. Eng.*, 127(2), 167–170.

Blanckaert, K. (2002). "Flow and turbulence in sharp open-channel bends." PhD thesis Nr 2545, Ecole Polytechnique Fédérale Lausanne, Switzerland.

Blanckaert, K., and de Vriend, H. J. (2003). "Nonlinear modeling of mean flow redistribution in curved open channels." *Water Resour. Res.*, 39(12), 6-1–6-14.

Blanckaert, K., and de Vriend, H. J. (2004). "Secondary flow in sharp open-channel bends." *J. Fluid Mech.*, 39, 353–380.

Blanckaert, K., Glasson, L., Jagers, H. R. A., and Sloff, C. J. (2003). "Quasi-3D simulation of flow in sharp open-channel bends with horizontal and developed bed topography." Proc., Int. Symp. Shallow Flows, Vol. I, Technical Univ. of Delft, Delft, The Netherlands, 93–100.

Blanckaert, K., and Graf, W. H. (2004). "Momentum transport in sharp open-channel bends." *J. Hydraul. Eng.*, 130(3), 186–198.

de Vriend, H. J. (1981). "Steady flow in shallow channel beds." *Communications on Hydraulics, Rep. No. 81-3*, Delft Univ. of Technology, Dept. of Civil Engineering, Delft, The Netherlands.

de Vriend, H. J., and Koch, F. G. (1977). "Flow of water in a curved open channel with a fixed plan bed." *Report on Experimental and Theoretical Investigations, Rep. No. R675-VM1415*, Part I, Delft Univ. of Technology, Delft, The Netherlands.

Johannesson, H., and Parker, G. (1989). "Velocity redistribution in meandering rivers." *J. Hydraul. Eng.*, 115(8), 1019–1039.

J. Hydraul. Eng. 2005.131:628-628.

Olesen, K. W. (1987). "Bed topography in shallow river bends." PhD thesis, *Rep. No. 87-1*, Dept. of Civil Engineering, Delft Univ. of Technology, Delft, The Netherlands.

Closure to "Investigation on the Suitability of Two-Dimensional Depth-Averaged Models for Bend-Flow Simulation" by T. Y. Hsieh and J. C. Yang

August 2003, Vol. 129, No. 8, pp. 597–612.
DOI: 10.1061/(ASCE)0733-9429(2003)129:8(597)

T. Y. Hsieh[1] and J. C. Yang[2]

[1]Research Assistant Professor, Natural Hazard Mitigation Research Center, National Chiao Tung Univ., Hsinchu, Taiwan. E-mail: tyhsieh.cv86g@nctu.edu.tw

[2]Professor, Dept. of Civil Engineering and Natural Hazard Mitigation Research Center, National Chiao Tung Univ., Hsinchu, Taiwan. E-mail: jcyang@mail.nctu.edu.tw

The writers thank the discusser for his comments and the reply is given in the following.

The discusser's opinions are based on velocity measurements in a sharp curved single-bend laboratory flume (Blanckaert 2004a). The writers would like to point out that the proposed model in the paper will not be applicable for the case with sharp curve. The limitation of the proposed model has been analyzed by the writers (Hsieh and Yang 2003). Therefore, although the writers mostly agree with the opinions from the discusser, some different opinions will be addressed as follows:

1. In the experiment by Blanckaert (2001), the flume can be regarded as a sharp curved channel, in which the radius of curvature, 2 m, is small compared with the width, 0.4 m, and a reverse secondary eddy is observed near the water surface at the outer bank. In fact, these flow conditions would not conform to the assumption of de Vriend's (1977) velocity profile adopted in the writers' model. So the dispersion stresses computed by the writers' model are inevitably different from the discusser's measured data. However, de Vriend (1977), de Vriend and Koch (1977) and Lien et al. (1999) have verified the applicability of the proposed velocity profile by several experimental results with mild curvature and single secondary eddy. As far as the numerical view point is concerned, the use of the velocity profile by de Vriend (1977) may still be a feasible technique for a two-dimensional (2D) depth-averaged model used to study the secondary current effect in a mild curved bend with a single secondary eddy.
2. As pointed out by the discusser, neglecting the feedback effects in the dispersion stress model may cause the overestimation of secondary flow effects, which can be as large as an order of magnitude for sharp bends. However, the magnitude of the overestimation for a moderately sharp curved channel, which is simulated in the writers' paper, is still not clear yet; further study may be needed. As long as the theoretical basis is maturely developed, the correction factor for the feedback effects can be embedded easily as far as the model development is concerned.
3. As pointed out by the discusser, in the case of the discusser's strongly curved experiment, the velocity distribution from the bend model may be overestimated compared to the measured data. However, one can observe from Figs. 2 and 3 in the discussion paper that the conventional model overestimated and underestimated the velocity distribution near the bend entrance and the exit respectively. This means that the secondary flow still plays a role to affect the flow pattern for the case of the strongly curved flow over developed bed topography. Hence, it may not be appropriate to state that a conventional model yields acceptable results for strongly curved flow over developed bed topography.

References

Blanckaert, K. (2001). "Discussion of 'Bend-flow simulation using 2D depth-averaged model' by H. C. Lien, et al.." *J. Hydraul. Eng.* 127(2), 167–170.

Blanckaert, K., and de Vriend, H. J. (2004). "Discussion of 'Investigation on the suitability of 2D depth-averaged models for bend-flow simulation' by T. Y. Hsieh and J. C. Yang." *J. Hydraul. Eng.*, 131(7), 625–628.

de Vriend, H. J. (1977). "Mathematical model of steady flow in curved shallow channels." *J. Hydraul. Res.*, 15(1), 37–54.

de Vriend, H. J., and Koch, F. G. (1977). "Flow of water in a curved open channel with a fixed plan bed." *Rep. on Experimental and Theoretical Investigations R675-VM1415, Part I*, Delft Univ. of Technology, Delft, The Netherlands.

Hsieh, T. Y., and Yang, J. C. (2003). "Investigation on the Suitability of 2D depth-averaged models for bend-flow simulation." *J. Hydraul. Eng.*. 129(8), 597–612.

Lien, H. C., Hsieh, T. Y., Yang, J. C., and Yeh, K. C. (1999). "Bend-flow simulation using 2D depth-averaged model." *J. Hydraul. Eng.*, 125(10), 1097–1108.

J. Hydraul. Eng. 2005.131:628-628.